Dalton Transactions

ROYAL SOCIETY OF CHEMISTRY

PAPER

View Article Online
View Journal | View Issue

Check for updates

Cite this: *Dalton Trans.*, 2025, **54**, 9761

Oxygen-modified Ru for efficient alkaline hydrogen evolution reaction†

Youpeng Cao, [a] Xingshuai Lv,[a] Jiao Yang,[a] Keyu An,[a] Chunfa Liu,[a] Lulu Qiao,[a] Zhichao Yu,[a] Lun Li[a] and Hui Pan *[a,b]

Received 8th April 2025,
Accepted 14th May 2025

DOI: 10.1039/d5dt00838g

rsc.li/dalton

Ruthenium (Ru) is considered a highly promising catalyst for the hydrogen evolution reaction (HER) because of its similar d-band center to platinum and more affordable price. However, the catalytic activities of Ru-based materials remain insufficient for large-scale water electrolysis. In this work, we report that an oxygen-modified Ru catalyst (Ru/C-220) can achieve superior catalytic performance for the HER with an overpotential of 18 mV at 10 mA cm^{-2}, a Tafel slope of 34.9 mV dec^{-1}, and around five-fold increase in mass activity at an overpotential of 100 mV compared to the unannealed catalyst. XPS characterization reveals that the catalyst, after air annealing, exhibits a higher content of lattice-O^{2-} and tetravalent ruthenium (Ru^{4+}), which are key factors contributing to performance enhancement. The underpotential-deposited hydrogen (H_{upd}) tests and density-functional-theory (DFT) calculations further validate that the enhanced performance of Ru/C-220 stems from oxygen modification, which reduces and optimizes the *H adsorption energy at the Ru active sites. Anion exchange membrane water electrolysis (AEMWE) tests confirm the application potential of the oxygen-modified Ru.

1. Introduction

The transition from traditional fossil fuels to hydrogen energy is widely regarded as one of the most important approaches for relieving the energy crisis and climate change.[1–3] Large-scale production of green hydrogen, as a prerequisite for a hydrogen society, is currently a research hotspot.[4,5] Anion and proton exchange membrane water electrolysis (AEMWE and PEMWE) processes are important technologies capable of achieving the industrial production of green hydrogen.[6] In particular, AEMWE operates under alkaline conditions, making the catalyst relatively more corrosion-resistant and able to exhibit fast oxygen evolution reaction (OER) kinetics.[7,8] However, AEMWE also faces a significant drawback: slow hydrogen evolution reaction (HER) kinetics, where substantial amounts of precious metal catalysts are needed, leading to high cost.[9] Therefore, developing electrocatalysts with low cost and high activity for the HER in AEMWE is crucial for energy transitions.[10–12]

Platinum (Pt) is widely recognized as an efficient catalyst for the HER. However, its high cost remains a limitation for commercial utilization on a large scale. In addition, Pt shows sluggish kinetics in alkaline electrolytes although it is highly active in acids. Accordingly, alternative materials are being widely explored to optimize water electrolysis in alkaline electrolytes. Ruthenium (Ru) has garnered increasing attention due to its higher catalytic activity for the alkaline HER compared to Pt, coupled with its relatively lower cost. Over the past decade, various Ru-based catalysts, including phosphides,[13–17] nitrides,[18,19] sulfides,[20,21] selenides[22–24] and heterojunction catalysts,[25–27] have been investigated for the alkaline HER. For example, Liu *et al.* developed a novel hybrid ruthenium–cobalt phosphide (RuCoP) cluster catalyst, achieving superior acidic and alkaline HER performance compared to commercial Pt/C catalysts.[28] Guo *et al.* significantly enhanced the catalytic activity of Ru for the alkaline HER by creating heterojunction structures through copper doping and selenation.[29] Similarly, Sun and co-workers reported a strongly coupled Ru–CrO_x cluster–cluster heterostructure with a unique interface between Ru and CrO_x, which could significantly reduce the energy barrier for breaking the H–OH bond to accelerate water dissociation.[30] Additionally, Huang *et al.* discovered that a snow-like Ru catalyst exhibits high catalytic activity for the alkaline HER.[25] Furthermore, active sites such as Ru–O–S, O–Ru–S, and O–Ru–N have shown high activity for the HER across the entire pH range.[31–33] The design of the catalyst support also plays a critical role in significantly enhancing its performance. In particular, loading ruthenium onto a carrier comprising a porous two-dimensional nitrogen-doped carbon

[a]*Institute of Applied Physics and Materials Engineering, University of Macau, Macao SAR, 999078, China. E-mail: huipan@um.edu.mo*
[b]*Department of Physics and Chemistry, Faculty of Science and Technology, University of Macau, Macao SAR, 999078, China*

† Electronic supplementary information (ESI) available. See DOI: https://doi.org/10.1039/d5dt00838g

structure (Ru@C_2N) enables a highly efficient HER across the full pH range.[34] Despite these advancements, the activity of Ru-based catalysts in the alkaline HER remains below expectations, and the methods for enhancing performance through synthesis are often overly intricate, posing challenges for large-scale implementation.[35,36] Therefore, it is essential to develop simple and broadly applicable approaches for further enhancing the performance, elucidating the mechanisms driving activity improvements, and assessing the potential for practical applications of Ru-based catalysts in the alkaline HER.

Herein, we report a facile method to improve the HER activity of Ru in alkaline electrolytes. An oxygen-modified Ru catalyst (Ru/C-220) was obtained by simple annealing of Ru/C in air. The Ru/C-220 exhibits superior electrocatalytic performance for the HER with an overpotential of 18 mV at 10 mA cm^{-2}, a Tafel slope of 34.9 mV dec^{-1}, and around a five-fold increase in mass activity at an overpotential of 100 mV compared to the unannealed catalyst. XPS characterization reveals that the catalyst, after air annealing, exhibits a higher content of lattice-O^{2-} and Ru^{4+}, which are key factors contributing to the performance enhancement. The underpotential-deposited hydrogen (H_{upd}) tests and density-functional-theory (DFT) calculations further confirm that the improved performance of Ru/C-220 is due to the reduced and optimized *H adsorption energy on oxygen-modified Ru. Anion exchange membrane water electrolysis (AEMWE) tests confirm the application potential of the oxygen-modified Ru. This work highlights that a simple air annealing method can significantly improve the catalytic activity of Ru in the alkaline HER.

2. Experimental section

2.1 Chemicals

Triruthenium dodecacarbonyl ($Ru_3(CO)_{12}$, >98%) was purchased from Bidepharm. Nafion perfluorinated resin solution (5 wt%) was purchased from Sigma Aldrich. Oleylamine ($C_{18}H_{37}N$, 80%–90%) was purchased from Macklin. Commercial Pt/C (20 wt% Pt) was purchased from Tanaka. Ethanol (C_2H_6O, AR), hexamethylene (C_6H_{12}, AR), isopropanol (C_3H_8O, AR) and potassium hydroxide (KOH, AR) were purchased from Aladdin. Vulcan carbon XC-72R was purchased from Cabot. All the chemicals were used without further purification. The deionized water (18 MΩ cm^{-1}) used in all the experiments was obtained by passing through an ultra-pure purification system (Aqua Solutions).

2.2 Materials synthesis

Synthesis of Ru nanocrystals and Ru/C. In a typical synthesis of Ru nanocrystals, 21 mg of $Ru_3(CO)_{12}$ and 5 mL of oleylamine were added into a glass vial (30 mL) and ultrasonicated for 0.5 h to form a homogeneous solution. The mixture was then heated to 200 °C and held at this temperature for 6 h in an oven. After cooling down to room temperature, the reaction mixture was washed with a mixture of ethanol/cyclohexane 3 times. The as-obtained nanocrystals in cyclohexane were added with 12 mg of XC-72R in ethanol and the mixture was ultrasonicated for 1 h.

Synthesis of Ru/C-200. Ru/C-200 was prepared by annealing Ru/C at 200 °C in air for 1 h.

Synthesis of Ru/C-220. Ru/C-220 was prepared by annealing Ru/C at 220 °C in air for 1 h.

Synthesis of Ru/C-240. Ru/C-240 was prepared by annealing Ru/C at 240 °C in air for 1 h.

Synthesis of NiFe LDH@Ni felt. A Ni felt substrate (dimensions: 10 × 10 × 0.3 mm^3) underwent surface purification through sequential exposure to 2 M acetic acid (to eliminate oxide layers) followed by 10-minute ultrasonication in ethanol and deionized water. NiFe-layered double hydroxide (LDH) was prepared by modifying an established procedure.[37,38] A mixture was formulated by dissolving 0.5 mmol Ni$(NO_3)_2{\cdot}6H_2O$, 0.5 mmol $Fe(NO_3)_3{\cdot}9H_2O$, and 5 mmol $CO(NH_2)_2$ in 36 mL of deionized water, and stirring it until fully uniform. The pre-treated Ni felt was submerged in this solution inside a 50 mL Teflon-lined stainless-steel autoclave, subjected to heating at 120 °C for 12 hours, and subsequently allowed to cool naturally to ambient temperature. The Ni felt, now coated with LDH, was washed with deionized water and ethanol, and then dried in a vacuum oven at 60 °C for 6 hours.

For the materials characterization of the samples, their electrochemical measurements and computational details of the calculations, see the ESI.†

3. Results and discussion

3.1 Synthesis and characterization

The Ru/C-220 catalyst was prepared by a two-step method. The Ru nanocrystals were first synthesized using $Ru_3(CO)_{12}$ (triruthenium dodecacarbonyl) as the metal precursor, and oleylamine (OAm) as the solvent and surfactant. When the reaction began, carbon monoxide was released from $Ru_3(CO)_{12}$, and Ru precipitated from the solution. The obtained Ru was loaded onto carbon black, which was annealed at 220 °C in air for one hour. Then, the final catalyst (Ru/C-220) was obtained. Transmission electron microscopy (TEM), Raman spectroscopy, electron paramagnetic resonance (EPR) spectroscopy, X-ray diffraction (XRD) and X-ray photoelectron spectroscopy (XPS) were performed to characterize the morphology and intrinsic structure of the as-synthesized catalyst.

The TEM images (Fig. 1a) show that the Ru nanocrystals exhibit irregular nanocluster morphology. After loading Ru onto carbon black and annealing in air, both the resulting Ru/C and Ru/C-220 catalysts exhibit similar nanocluster morphologies (Fig. S1†). The HRTEM image of Ru/C (Fig. 1a) shows the lattice distances of 0.218 and 0.235 nm, which are ascribed to Ru (002) and Ru (100) facets, respectively. The *d*-spacing of 0.246 nm is assigned to the (101) crystal plane of RuO_2 (Fig. 1b). Energy-dispersive X-ray spectroscopy (EDS) elemental mappings confirm the presence of oxygen in the catalyst and the uniform dispersion of Ru on carbon black (Fig. 1c). Both Ru/C-200 and Ru/C-240 (Fig. S2 and S3†) show

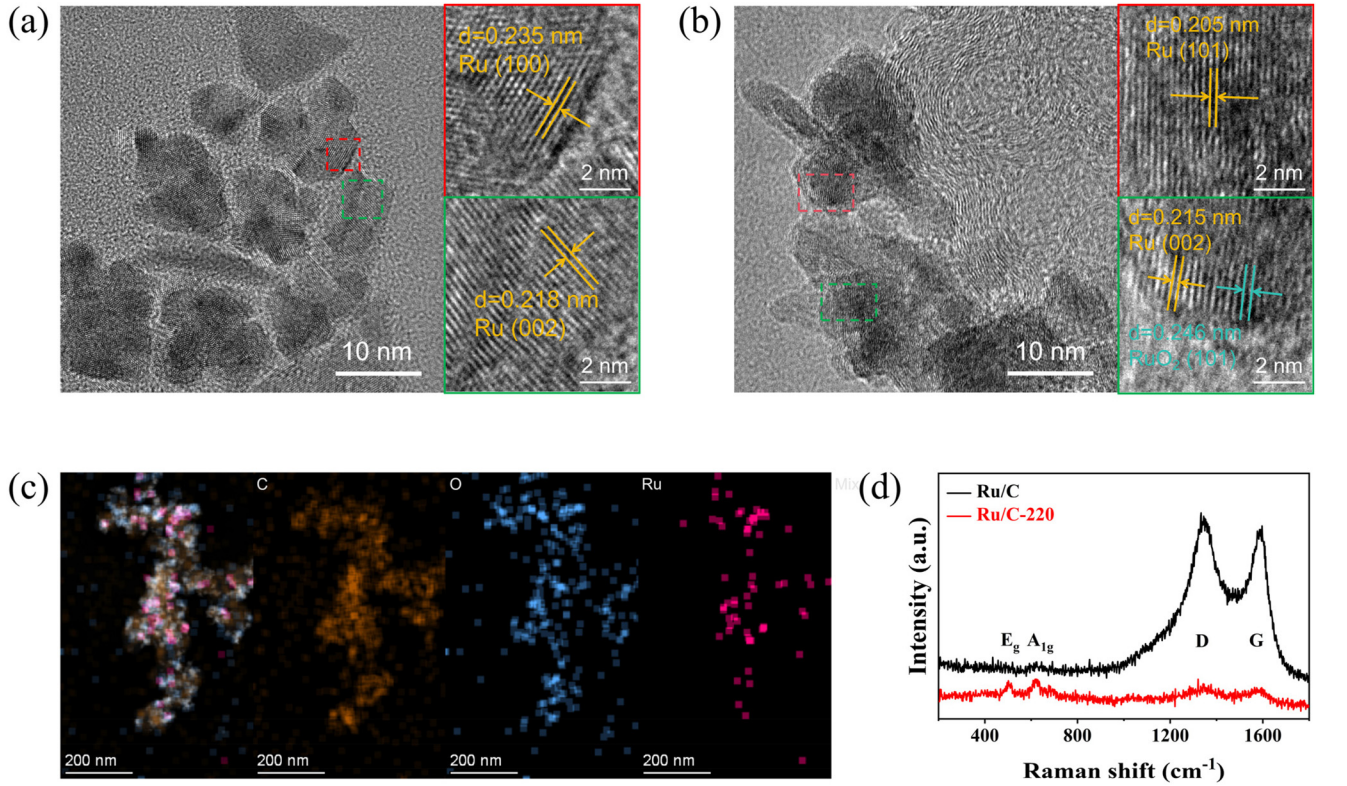

Fig. 1 Morphological characterization. HRTEM images of (a) Ru nanocrystals and (b) Ru/C-220. (c) EDS mapping of Ru/C-220, and (d) Raman spectra of Ru/C and Ru/C-220.

the same morphologies as Ru/C-220. The Raman spectra of Ru/C-220 (Fig. 1d) show two main peaks at 528 cm^{-1} and 644 cm^{-1}, which correspond to E_g and A_{1g} modes, respectively.[39] Ru/C without annealing shows no obvious E_g and A_{1g} modes.

The oxygen vacancies were confirmed by the characteristic electron paramagnetic resonance (EPR) signal *g*-factor = 2.004 (Fig. 2a), which is related to the oxygen vacancies.[40] As the annealing temperature of Ru/C increases, the density of oxygen vacancies decreases (Fig. S4†). The lattice-O^{2-} content in Ru/C-220 is much higher than that in Ru/C, as indicated by the reduced EPR signal, which is verified in the XPS analysis below. The X-ray diffraction (XRD) patterns of Ru/C-220 and Ru/C (Fig. 2b) show that the peaks at 38.38°, 42.15°, 44.00°, 58.32°, 69.41°, 78.39°, 84.70°, and 85.95° correspond to the Ru (100), (002), (101), (102), (110), (103), (112), and (201) crystal planes (JCPDS no. 06-0663), respectively. The peaks at 28.01°, 35.05° and 54.25° are related to the RuO_2 (110), (101) and (211) crystal planes (JCPDS no. 40-1290), respectively. The space group of Ru with an hcp structure is *P*63/*mmc* (194) and that of RuO_2 is *P*42/*mnm* (136). Therefore, the presence of the RuO_2 crystalline phase in the annealed Ru/C-220 is confirmed. The XRD results of Ru/C-220 (Fig. 2c) show that there is a compression of 2.03% and 0.60% for RuO_2 (101) and (211) crystal planes, respectively, because of the formation of RuO_2 crystals.[41] Comparing XRD results of the samples annealed at different temperatures reveals that as the annealing temperature increases (Fig. S5†), the content of crystalline RuO_2 increases, which reduces the HER activity of Ru/C-240.

The XPS full spectra of Ru/C and Ru/C-220 (Fig. S6†) confirm the existence of Ru, C and O in the samples without other impurities. The O 1s XPS spectra of Ru/C-220 and Ru/C (Fig. 2d) reveal three different O types, including the lattice-O^{2-} (at around 530.1 eV, O_{Lat}), the hydroxyl (HO) groups adsorbed to the metal atoms in the oxygen-deficient region (at around 531.4 eV, O_V), and the adsorbed water (at around 532.8 eV, O_{Abs}).[42–47] The peak intensity at 530.0 eV is higher than that at 531.5 eV for Ru/C-220, indicating the decrease of O_V and increase of O_{Lat} after the annealing. The Ru 3p XPS spectrum of Ru/C (Fig. 2e) shows that after annealing, the peak position of Ru $3p_{1/2}$ increases from 484.4 eV to 485.1 eV, and the peak position of Ru $3p_{3/2}$ increases from 462.2 eV to 462.9 eV, indicating an increase in the Ru^{4+} component.[48] From the Ru $3d_{5/2}$ XPS spectrum (Fig. 2f), the peak of Ru^{4+} $3d_{5/2}$ in Ru/C-220 shifts to a higher binding energy (281.2 eV) compared with that in Ru/C without annealing (281.0 eV) and the peak of Ru^0 $3d_{5/2}$ in Ru/C-220 shifts to lower binding energy (280.4 eV) compared with that in Ru/C without annealing (280.6 eV). The XPS spectra of Ru 3p and 3d (Fig. 2e and f) show clearly that Ru/C-220 exhibits a higher proportion of Ru^{4+} compared to Ru/C. The Ru^{4+}/Ru^0 area ratio in Ru/C is 0.50, which increases to 1.64 after annealing at 220 °C in air for one hour

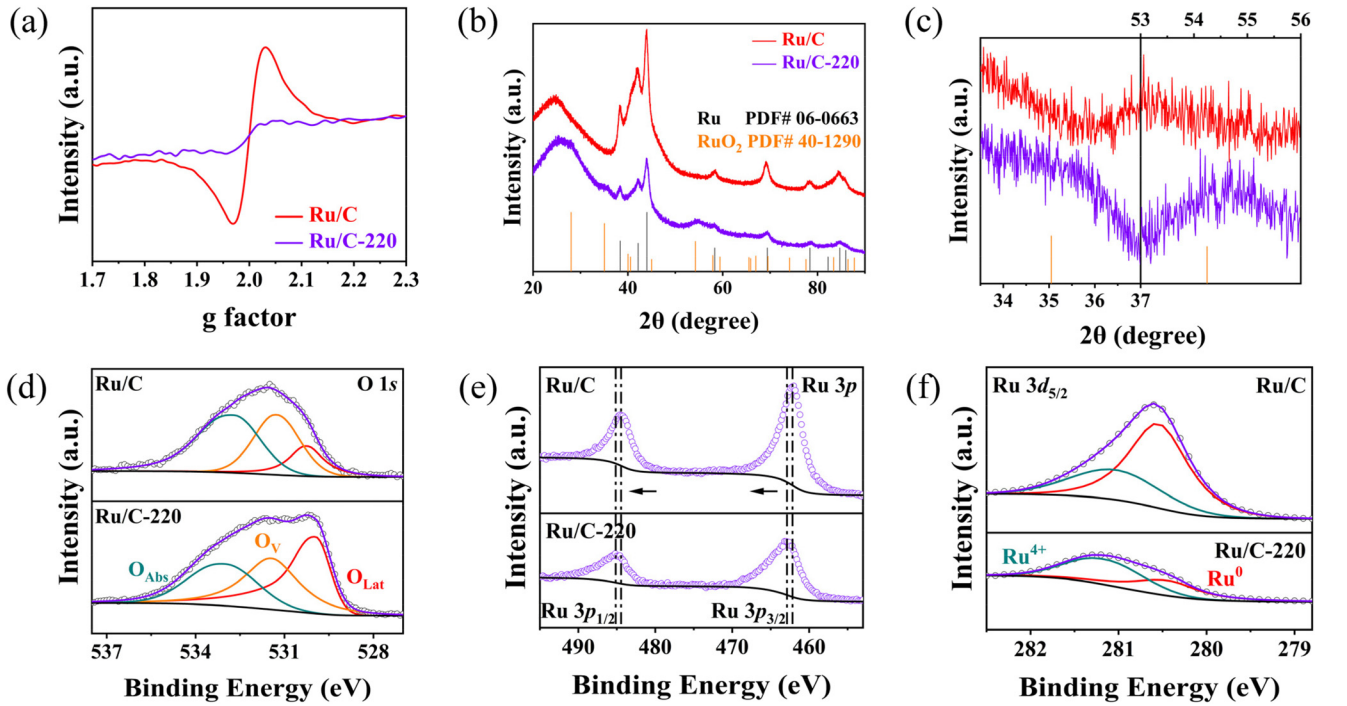

Fig. 2 (a) EPR spectra of Ru/C and Ru/C-220, (b) XRD patterns, and (c) high-resolution XRD patterns of Ru/C and Ru/C-220. High-resolution XPS spectra of Ru/C and Ru/C-220 for (d) O 1s, (e) Ru 3p, and (f) Ru 3d.

(Table S1†). The O_V/O_{Lat} ratio decreases from 2.25 to 0.89, which is consistent with the EPR characterization (Table S1†). Clearly, our TEM, Raman spectroscopy, EPR, XRD, and XPS analyses collectively indicate that Ru/C-220 predominantly exists in a metallic Ru crystal structure, and air annealing increases the oxygen content in Ru while reducing the density of oxygen vacancies, which is crucial to catalytic activity. Nevertheless, elevated annealing temperatures unavoidably promote the increased formation of crystalline RuO_2, leading to a substantial decline in the performance, as RuO_2 exhibits negligible HER activity (Fig. S7†).

3.2 HER performance

The HER performances of the as-synthesized Ru/C-220, Ru/C and commercial Pt/C were investigated in 1.0 M KOH. The Ru/C-220 exhibits the best HER activity performance with low overpotential (η) values of 18 mV and 87 mV at 10 and 100 mA cm^{-2}, respectively, much lower than those of Ru/C (54 mV at 10 mA cm^{-2}) and commercial Pt/C (36 mV at 10 mA cm^{-2}) (Fig. 3a). The LSV curves without *iR* correction show consistent results and are also presented (Fig. S8†). The HER activity of commercial Ru/C, and Ru/C oxidized at 240 °C (Ru/C-240) and at 200 °C (Ru/C-200) was also tested. The commercial Ru/C (99 mV) from Macklin, Ru/C-240 (63 mV) and Ru/C-200 (21 mV) all show higher overpotential values at 10 mA cm^{-2} than Ru/C-220 (Fig. S8†). Inductively coupled plasma-mass spectrometry (ICP-MS) analysis was performed, revealing the weight percentages of Ru in Ru/C and Ru/C-220 to be 28.4% and 29.2%, respectively. These values enable the calculation of the mass activity of catalysts. The mass activity of Ru/C-220 (3.75 A mg^{-1}) at the overpotential of 100 mV is 5.14 and 2.66 times as high as those values of Ru/C (0.73 A mg^{-1}) and commercial Pt/C (1.66 A mg^{-1}), respectively (Fig. 3b and Fig. S9†). Electrochemical impedance spectroscopy (EIS) was employed to further investigate the HER kinetics (Fig. 3c and Fig. S10†). The Nyquist plots of all samples show that the near-semicircle arises, which can be well fitted by an equivalent circuit model including R_s (solution resistance), R_{ct} (charge transfer resistance) and CPE (constant phase element). The fitting results (Table S3†) show that the solution resistances of all samples are around 5.1 Ω. The charge transfer resistances were found to be 16.3, 30.9, 5.8, 4.4 and 14.6 Ω for Pt/C, Ru/C, Ru/C-200, Ru/C-220 and Ru/C-240, respectively. The Ru/C-220 exhibits the lowest charge transfer resistance, corresponding to its superior HER performance.[49] The Tafel slopes were found to be 34.9, 46.4 and 56.2 mV dec^{-1} for Ru/C-220, commercial Pt/C, and Ru/C, respectively (Fig. 3d), suggesting that the rate-determining step switches from the sluggish Volmer step to the Tafel step for Ru/C-220.[50] Based on the overpotential at 10 mA cm^{-2} and the Tafel slope, our Ru/C-220 catalyst is one of the best state-of-the-art alkaline HER catalysts (Table S2†). The electrochemical double-layer capacitance (C_{dl}) of the catalyst was also determined (Fig. S11†). Since the powder consists of carbon black and metal, the C_{dl} value cannot be used to calculate the ECSA of the metal active sites. In addition, the Ru/C-220 shows good long-term stability with a performance degradation rate of only 0.139 mV h^{-1} at 10 mA cm^{-2} (Fig. 3e).

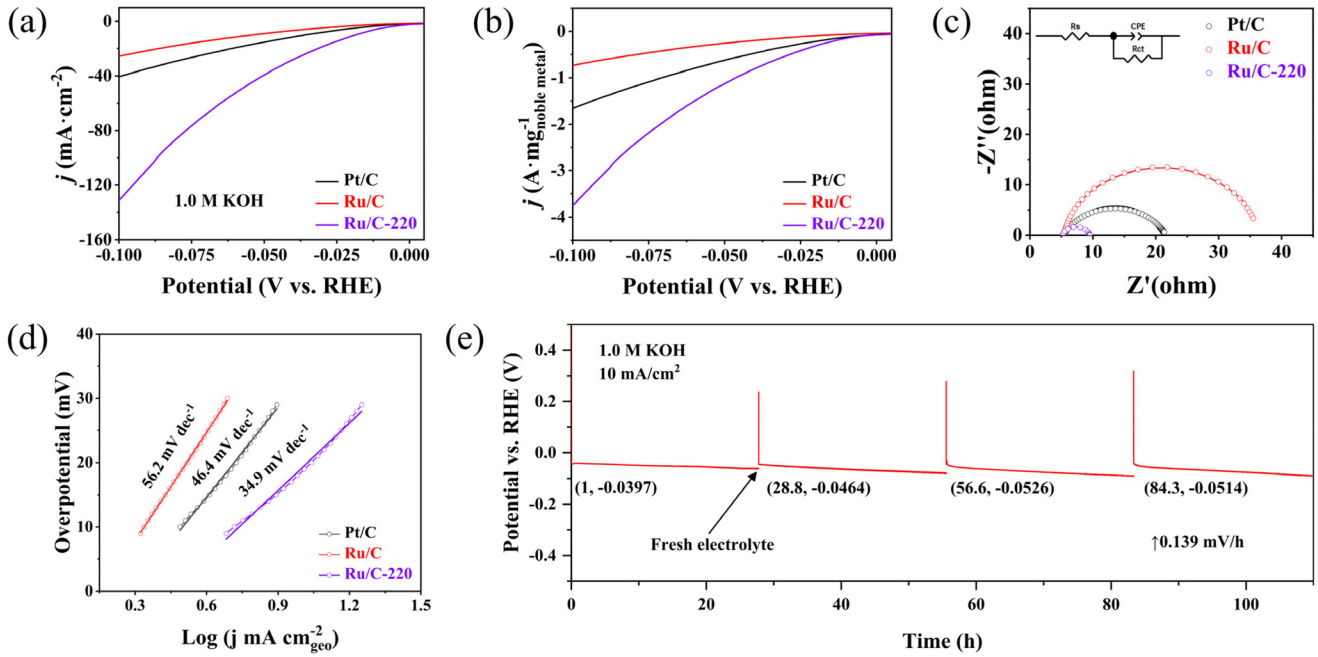

Fig. 3 (a) HER polarization curves in nitrogen-saturated 1 M KOH electrolyte with a rotating speed of 1600 rpm. (b) Mass-normalized HER polarization curves of different catalysts. (c) Electrochemical impedance spectra of Pt/C, Ru/C and Ru/C-220 from 100 kHz to 0.01 Hz (R_s: solution resistance, R_{ct}: charge transfer resistance, CPE: constant phase element; dotted lines show fitted curves; solid lines represent experimental data). (d) Tafel plots. (e) Chronopotentiometric curves of Ru/C-220 under alkaline conditions at 10 mA cm^{-2} without *iR* correction.

To further explore the mechanism for the improved activity of Ru/C-220, electrochemical methods, including CO-stripping (Fig. 4a) and copper underpotential deposition (Cu-UPD) (Fig. 4b), were employed.[41,51] From the CO-stripping tests, the potentials of the peak positions follow the order of Pt/C > Ru/C ≈ Ru/C-220, indicating Ru exhibits better resistance to CO

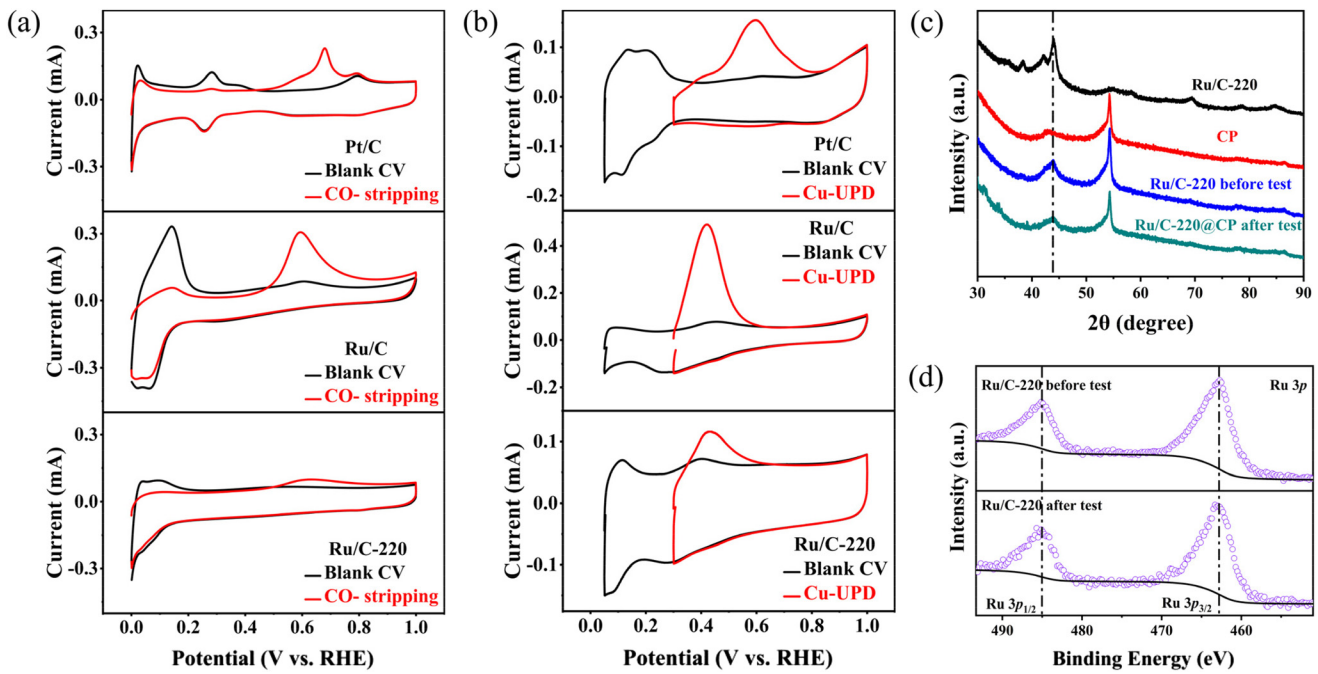

Fig. 4 (a) CVs and CO-stripping voltammograms of commercial Pt/C, Ru/C and Ru/C-220 catalysts. (b) CVs and Cu-UPD voltammograms of commercial Pt/C, Ru/C and Ru/C-220 catalysts. (c) XRD patterns of Ru/C-220, CP and Ru/C-220@CP before and after the stability test. (d) High-resolution XPS spectra of Ru/C-220 before and after the stability test for Ru 3p.

poisoning compared to Pt. The ECSA values were found to be 10.6, 41.3 and 58.2 $m^2\ g^{-1}$ for Ru/C-220, commercial Pt/C, and Ru/C, respectively, by CO-stripping (Fig. 4a). The ECSA values were found to be 11.6, 50.9 and 94.9 $m^2\ g^{-1}$ for Ru/C-220, commercial Pt/C, and Ru/C, respectively, by Cu-UPD (Fig. 4b). The lower ECSA of the oxidized Ru catalyst is due to the decreased adsorption capacity for carbon monoxide and copper ions on the catalyst surface, rather than an actual decrease in the ECSA. In many studies, CO-stripping and Cu-UPD are not used to measure the ECSA of oxidized Ru. Therefore, the ECSA of the oxygen-modified Ru catalyst prepared in our work cannot be accurately measured. Characterization before and after electrocatalytic reactions is crucial for understanding the electrocatalytic process. Therefore, we conducted TEM, XRD, and XPS characterization studies on the catalyst before and after stability testing. The TEM image (Fig. S12†) of Ru/C-220 was acquired after the stability test. The image shows that there were no significant morphological changes in the catalyst after the stability test. We compared Ru/C-220, carbon paper, Ru/C-220 loaded on carbon paper before stability testing, and Ru/C-220 loaded on carbon paper after stability testing. The results indicate that carbon paper exhibits very distinct diffraction peaks at 26.3° and 54.3°, and the diffraction peaks of the Ru metal showed no significant changes before and after stability testing (Fig. 4c). In the Ru 3p XPS spectra (Fig. 4d), no significant peak shift was observed before and after the stability test, further verifying the stability of the catalyst. Overall, the TEM, XRD and XPS characterization results before and after the stability test indicate that the catalyst exhibits good stability.

3.3 Mechanism investigation and AEMWE

To clarify the mechanisms driving the enhanced activity and practical potential of the Ru/C-220 catalyst, we performed a detailed study, encompassing underpotential-deposited hydrogen (H_{upd}) tests, DFT calculations, and anion exchange membrane water electrolysis (AEMWE) assessments.

Cyclic voltammetry (CV) experiments were conducted in a nitrogen-saturated 1 M KOH electrolyte at a scan rate of 100 mV s^{-1} to examine the electrochemical properties of Ru/C-200 and the mechanism for its improved HER performance. The data (Fig. 5a) demonstrate that the H_{upd} peak for Ru/C is significantly stronger than that for Ru/C-220, suggesting that Ru/C-220 exhibits weakened and optimized Ru–H binding energy. This attribute underpins its improved HER catalytic performance, while also aligning with recent investigations into hydrogen-binding energy mechanisms in the alkaline HER.[52] To further confirm the experimental result of the mechanism underlying the improved HER activity of Ru/C-220 in an alkaline electrolyte, we conducted DFT calculations.[25,53,54] Models representing the pristine and oxidized Ru (101) crystal plane were constructed (Fig. S13†). The calculated water adsorption energies (ΔE) are −0.68 eV for pristine Ru (101) and −0.89 eV for the oxidized Ru (101), indicating a stronger affinity for water on the latter (Fig. 5b). We calculated the Gibbs free energy of hydrogen adsorption (ΔG_H) since it is a crucial descriptor of HER activity (Fig. 5c). The ΔG_H value (0.11 eV) calculated for the oxidized Ru (101), being closer to 0 than −0.52 eV for pristine Ru, suggests that oxygen modifi-

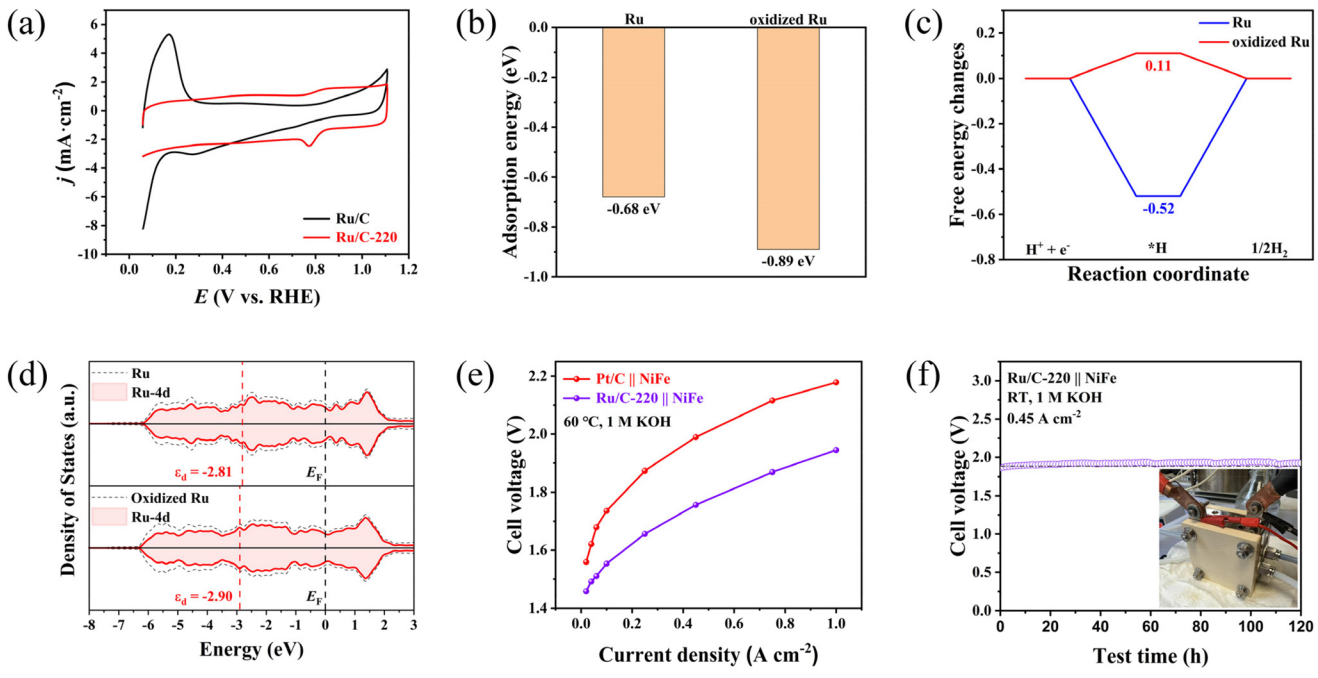

Fig. 5 (a) CV polarization curves of Ru/C and Ru/C-220 in N_2-saturated 1 M KOH solution with a scan rate of 100 mV s^{-1} at 1600 rpm. (b) The adsorption energies of H_2O on pristine Ru and oxidized Ru. (c) Free energy variations of *H adsorption on Ru and oxidized Ru. (d) The projected density of states (PDOS) of Ru and oxidized Ru. (e) Polarization curves of the AEMWE with Ru/C-220 and Pt/C as cathode catalysts without *iR* correction at 60 °C, respectively. (f) Chronopotentiometric data for the Ru/C-220-based AEMWE tested at 0.45 A cm^{-2} and room temperature.

cation effectively weakens and optimizes the inherently strong hydrogen binding of Ru, which facilitates the Tafel step of the HER. Moreover, partial density of states (PDOS) analysis (Fig. 5d) reveals a downshift in the d-band center of oxidized Ru (101) to −2.90 eV from −2.81 eV for the pristine Ru (101). This observation is consistent with the d-band center theory, which proposes that a lower d-band center optimizes the adsorption strength of Ru with reaction intermediates, explaining the observed change in the hydrogen-binding energy upon oxidation (from −0.52 eV to 0.11 eV) and the consequent improvement in HER activity.

The Ru/C-220 used as a cathode catalyst was incorporated into a membrane electrode assembly (MEA). The anode catalyst is NiFe-layered double hydroxide (LDH) supported on nickel felt. Current–voltage curves of the Ru/C-220-assembled AEMWE and reference Pt/C devices were measured at 60 °C in 1 M KOH electrolyte (Fig. 5e). The results show that the Ru/C-220-based AEMWE can achieve 0.45 A cm^{-2} and 1.0 A cm^{-2} current densities at low voltages of 1.756 V and 1.945 V, respectively, values that are significantly lower than the voltage required for the Pt/C-based device at the same current density (1.989 V at 0.45 A cm^{-2} and 2.179 V at 1.0 A cm^{-2}). In addition, Ru/C-220-AEMWE, after running continuously for 120 hours at 0.45 A cm^{-2}, maintained a voltage of 1.920 V, revealing good stability (Fig. 5f). Stability tests were performed at room temperature to reduce the leaching of iron from the NiFe LDH anode at high temperatures.[55–57] These results demonstrate the potential of Ru/C-220 for practical AEMWE applications.

4. Conclusions

In summary, we report a facile method to improve the HER activity of Ru in alkaline electrolytes. The oxygen-modified Ru catalyst (Ru/C-220) was obtained by a simple annealing of Ru/C in air. Ru/C-220 exhibits a superior electrocatalytic performance for the HER with an overpotential of 18 mV at 10 mA cm^{-2}, a Tafel slope of 34.9 mV dec^{-1}, and around a five-fold increase in mass activity at an overpotential of 100 mV compared to the unannealed catalyst. XPS characterization reveals that the catalyst after air annealing exhibits a higher content of lattice-O^{2-} and Ru^{4+}, which are key factors contributing to the performance enhancement. H_{upd} tests and DFT calculations further validate that the enhanced performance of Ru/C-220 stems from oxygen modification, which reduces and optimizes the *H adsorption energy at the Ru active sites. AEMWE tests confirm the application potential of the oxygen-modified Ru. This work highlights that a simple air annealing method can significantly improve the catalytic activity of Ru in the alkaline HER.

Author contributions

Youpeng Cao: conceptualization, formal analysis, investigation, methodology, and writing – original draft. Xingshuai Lv: conceptualization, formal analysis, investigation, and software. Jiao Yang: formal analysis, investigation and methodology. Keyu An: formal analysis, investigation, and methodology. Chunfa Liu: formal analysis, investigation, and methodology. Lulu Qiao: formal analysis and writing – review and editing. Zhichao Yu: formal analysis. Lun Li: formal analysis. Hui Pan: formal analysis, funding acquisition, project administration, supervision, and writing – review and editing.

Data availability

The data supporting this article have been included as part of the ESI.†

Conflicts of interest

The authors declare no conflict of interest.

Acknowledgements

This work was supported by the Science and Technology Development Fund (FDCT) from Macau SAR (0050/2023/RIB2, 0023/2023/AFJ, 006/2022/ALC, and 0111/2022/A2), Multi-Year Research Grants (MYRG-GRG2023-00010-IAPME and MYRG2022-00026-IAPME) from the Research & Development Office at the University of Macau, and the Shenzhen–Hong Kong–Macao Science and Technology Research Programme (Type C) (SGDX20210823103803017) from Shenzhen.

References

1 W. A. Braff, J. M. Mueller and J. E. Trancik, *Nat. Clim. Change*, 2016, **6**, 964–969.
2 S. Chu and A. Majumdar, *Nature*, 2012, **488**, 294–303.
3 J. K. Norskov, T. Bligaard, A. Logadottir, J. R. Kitchin, J. G. Chen and S. Pandelov, *J. Electrochem. Soc.*, 2005, **152**, J23–J26.
4 J. A. Turner, *Science*, 2004, **305**, 972–974.
5 P. F. Zhou, H. Y. Bai, J. X. Feng, D. Liu, L. L. Qiao, C. F. Liu, S. P. Wang and H. Pan, *J. Mater. Chem. A*, 2023, **11**, 1551–1574.
6 H. A. Miller, K. Bouzek, J. Hnat, S. Loos, C. I. Bernäecker, T. Weissgärber, L. Röntzsch and J. Meier-Haack, *Sustainable Energy Fuels*, 2020, **4**, 2114–2133.
7 M. P. Chen, D. Liu, J. X. Feng, P. F. Zhou, L. L. Qiao, W. L. Feng, Y. Y. Chen, K. W. Ng, S. P. Wang, W. F. Ip and H. Pan, *Chem. Eng. J.*, 2022, **443**, 136432.
8 C. F. Liu, J. X. Feng, P. F. Zhou, D. Liu, L. L. Qiao, Y. P. Cao, S. C. Su, H. C. Liu and H. Pan, *Chem. Eng. J.*, 2023, **476**, 146710.
9 J. Durst, C. Simon, F. Hasché and H. A. Gasteiger, *J. Electrochem. Soc.*, 2015, **162**, F190–F203.

10 J. Greeley, T. F. Jaramillo, J. Bonde, I. B. Chorkendorff and J. K. Norskov, *Nat. Mater.*, 2006, **5**, 909–913.
11 Y. Jiao, Y. Zheng, M. T. Jaroniec and S. Z. Qiao, *Chem. Soc. Rev.*, 2015, **44**, 2060–2086.
12 Z. W. Seh, J. Kibsgaard, C. F. Dickens, I. B. Chorkendorff, J. K. Norskov and T. F. Jaramillo, *Science*, 2017, **355**, eaad4998.
13 Q. B. Chang, J. W. Ma, Y. Z. Zhu, Z. Li, D. Y. Xu, X. Z. Duan, W. C. Peng, Y. Li, G. L. Zhang, F. B. Zhang and X. B. Fan, *ACS Sustainable Chem. Eng.*, 2018, **6**, 6388–6394.
14 D. Chen, Z. H. Pu, R. H. Lu, P. X. Ji, P. Y. Wang, J. W. Zhu, C. Lin, H. W. Li, X. G. Zhou, Z. Y. Hu, F. J. Xia, J. S. Wu and S. C. Mu, *Adv. Energy Mater.*, 2020, **10**, 2000814.
15 D. H. Li, R. S. Cai, D. Y. Zheng, J. Ren, C. L. Dong, Y. C. Huang, S. J. Haigh, X. Liu, F. L. Gong, Y. M. Liu, J. Liu and D. J. Yang, *Adv. Sci.*, 2024, **11**, 2309869.
16 J. Y. Zhao, Y. Y. Zhang, Y. Xia, B. Zhang, Y. C. Du, B. Song, H. L. Wang, S. W. Li and P. Xu, *Appl. Catal., B*, 2023, **328**, 122447.
17 S. Z. Zhou, H. Jang, Q. Qin, L. Q. Hou, M. G. Kim, S. G. Liu, X. E. Liu and J. Cho, *Angew. Chem.*, 2022, **134**, e202212196.
18 J. N. Tiwari, A. M. Harzandi, M. Ha, S. Sultan, C. W. Myung, H. J. Park, D. Y. Kim, P. Thangavel, A. N. Singh, P. Sharma, S. S. Chandrasekaran, F. Salehnia, J. W. Jang, H. S. Shin, Z. Lee and K. S. Kim, *Adv. Energy Mater.*, 2019, **9**, 1900931.
19 S. Y. Yun, S. Lee, X. Jin, A. Soon and S. J. Hwang, *Adv. Sci.*, 2024, **11**, 2309819.
20 P. S. Li, X. X. Duan, S. Y. Wang, L. R. Zheng, Y. P. Li, H. H. Duan, Y. Kuang and X. M. Sun, *Small*, 2019, **15**, 1904043.
21 J. W. Zhu, Y. Guo, F. Liu, H. W. Xu, L. Gong, W. J. Shi, D. Chen, P. Y. Wang, Y. Yang, C. T. Zhang, J. S. Wu, J. H. Luo and S. C. Mu, *Angew. Chem., Int. Ed.*, 2021, **60**, 12328–12334.
22 D. Chen, R. H. Lu, Y. T. Yao, D. L. Wu, H. Y. Zhao, R. H. Yu, Z. H. Pu, P. Y. Wang, J. W. Zhu, J. Yu, P. X. Ji, Z. K. Kou, H. L. Tang and S. C. Mu, *J. Mater. Chem. A*, 2022, **10**, 7637–7644.
23 R. Qin, P. Y. Wang, Z. L. Li, J. X. Zhu, F. Cao, H. W. Xu, Q. L. Ma, J. Y. Zhang, J. Yu and S. C. Mu, *Small*, 2022, **18**, 2105305.
24 K. F. Wang, B. Li, W. Wei, J. G. Wang, Q. Shen and P. Qu, *Nanoscale*, 2020, **12**, 23740–23747.
25 J. T. Zhang, G. M. Ren, D. Y. Li, Q. Y. Kong, Z. W. Hu, Y. Xu, S. L. Wang, L. Wang, M. F. Cao and X. Q. Huang, *Sci. Bull.*, 2022, **67**, 2103–2111.
26 W. Y. Tian, X. Xie, X. A. Zhang, J. H. Li, G. I. N. Waterhouse, J. Ding, Y. S. Liu and S. Y. Lu, *Small*, 2024, **20**, 2309633.
27 T. Q. Yu, Q. L. Xu, L. Luo, C. R. Liu and S. B. Yin, *Chem. Eng. J.*, 2022, **430**, 133117.
28 J. Xu, T. Liu, J. Li, B. Li, Y. Liu, B. Zhang, D. Xiong, I. Amorim, W. Li and L. Liu, *Energy Environ. Sci.*, 2018, **11**, 1819–1827.
29 K. Wang, J. H. Zhou, M. Z. Sun, F. X. Lin, B. L. Huang, F. Lv, L. Y. Zeng, Q. H. Zhang, L. Gu, M. C. Luo and S. J. Guo, *Adv. Mater.*, 2023, **35**, 2300980.
30 B. X. Zhang, J. M. Wang, G. M. Liu, C. M. Weiss, D. Q. Liu, Y. P. Chen, L. X. Xia, P. Zhou, M. X. Gao, Y. F. Liu, J. Chen, Y. S. Yan, M. H. Shao, H. G. Pan and W. P. Sun, *Nat. Catal.*, 2024, **7**, 441–451.
31 D. Guo, X. Xue, M. Jiao, J. Liu, T. Wu, X. Ma, D. Lu, R. Zhang, S. Zhang, G. Shao and Z. Zhou, *Chem. Sci.*, 2024, **15**, 16281–16290.
32 Z. Han, S. Son, K. Kim, S. Gao and G. Shao, *Chem. Mater.*, 2024, **36**, 1831–1840.
33 G. Shao, J. Xu, S. Gao, Z. Zhang, S. Liu, X. Zhang and Z. Zhou, *Carbon Energy*, 2024, **6**, e417.
34 J. Mahmood, F. Li, S. Jung, M. Okyay, I. Ahmad, S. Kim, N. Park, H. Jeong and J. Baek, *Nat. Nanotechnol.*, 2017, **12**, 441–446.
35 X. Li, D. Fang, J. Yi, L. Zhang, J. Liu and F. Liu, *Dalton Trans.*, 2024, **53**, 18549–18559.
36 M. Sadangi, C. Chakravarty, J. Bhattacharjee and J. Behera, *Dalton Trans.*, 2024, **53**, 16384–16396.
37 Z. Lu, W. Xu, W. Zhu, Q. Yang, X. Lei, J. Liu, Y. Li, X. Sun and X. Duan, *Chem. Commun.*, 2014, **50**, 6479–6482.
38 Q. Xiang, F. Li, W. Chen, Y. Ma, Y. Wu, X. Gu, Y. Qin, P. Tao, C. Song, W. Shang, H. Zhu, T. Deng and J. Wu, *ACS Energy Lett.*, 2018, **3**, 2357–2365.
39 S. Y. Mar, C. S. Chen, Y. S. Huang and K. K. Tiong, *Appl. Surf. Sci.*, 1995, **90**, 497–504.
40 J. D. Chen, C. H. Chen, M. K. Qin, B. Li, B. B. Lin, Q. Mao, H. B. Yang, B. Liu and Y. Wang, *Nat. Commun.*, 2022, **13**, 5382.
41 M. C. Luo, Z. L. Zhao, Y. L. Zhang, Y. J. Sun, Y. Xing, F. Lv, Y. Yang, X. Zhang, S. Hwang, Y. N. Qin, J. Y. Ma, F. Lin, D. Su, G. Lu and S. J. Guo, *Nature*, 2019, **574**, 81–85.
42 V. H. Do, P. Prabhu, V. Jose, T. Yoshida, Y. T. Zhou, H. Miwa, T. Kaneko, T. Uruga, Y. Iwasawa and J. M. Lee, *Adv. Mater.*, 2023, **35**, 2208860.
43 G. Li, H. Jang, S. Liu, Z. Li, M. Kim, Q. Qin, X. Liu and J. Cho, *Nat. Commun.*, 2022, **13**, 1270.
44 Y. Shen, X. Zhang, M. Qu, J. Ma, S. Zhu, Y. Min, M. Gao and S. Yu, *Nat. Commun.*, 2024, **15**, 7861.
45 J. Tang, D. Guan, H. Xu, L. Zhao, U. Arshad, Z. Fang, T. Zhu, M. Kim, C. Pao, Z. Hu, J. Ge and Z. Shao, *Nat. Commun.*, 2025, **16**, 801.
46 Y. Wen, C. Liu, R. Huang, H. Zhang, X. Li, F. de Arquer, Z. Liu, Y. Li and B. Zhang, *Nat. Commun.*, 2022, **13**, 4871.
47 G. Zhao, W. Guo, M. Shan, Y. Fang, G. Wang, M. Gao, Y. Liu, H. Pan and W. Sun, *Adv. Mater.*, 2024, **36**, 2404213.
48 X. K. Wu, Z. C. Wang, D. Zhang, Y. N. Qin, M. H. Wang, Y. Han, T. R. Zhan, B. Yang, S. X. Li, J. P. Lai and L. Wang, *Nat. Commun.*, 2021, **12**, 4018.
49 X. F. Bai, X. P. Zhang, Y. J. Sun, M. C. Huang, J. T. Fan, S. Y. Xu and H. Li, *Angew. Chem., Int. Ed.*, 2023, **62**, e202308704.
50 C. Z. Wan, Z. S. Zhang, J. C. Dong, M. J. Xu, H. T. Pu, D. Baumann, Z. Y. Lin, S. B. Wang, J. Huang, A. H. Shah,

X. Q. Pan, T. D. Hu, A. N. Alexandrova, Y. Huang and X. F. Duan, *Nat. Mater.*, 2023, **22**, 1022–1029.
51 J. L. Gu, L. X. Li, Y. E. Xie, B. Chen, F. B. Tian, Y. J. Wang, J. Zhong, J. D. Shen and J. Lu, *Nat. Commun.*, 2023, **14**, 5389.
52 H. Li, C. Tsai, A. Koh, L. Cai, A. Contryman, A. Fragapane, J. Zhao, H. Han, H. Manoharan, F. Abild-Pedersen, J. Norskov and X. Zheng, *Nat. Mater.*, 2016, **15**, 48–53.
53 Y. P. Li, W. T. Wang, M. Y. Cheng, Y. F. Feng, X. Han, Q. Z. Qian, Y. Zhu and G. Q. Zhang, *Adv. Mater.*, 2023, **35**, 2206351.
54 J. T. Zhang, X. N. Mao, S. L. Wang, L. L. Liang, M. F. Cao, L. Wang, G. Li, Y. Xu and X. Q. Huang, *Angew. Chem., Int. Ed.*, 2022, **61**, e202116867.
55 X. Cui, T. Tang, F. Zhang, L. Sun and B. Zhang, *Appl. Catal., B*, 2025, **366**, 125024.
56 Z. Li, G. Lin, L. Wang, H. Lee, J. Du, T. Tang, G. Ding, R. Ren, W. Li, X. Cao, S. Ding, W. Ye, W. Yang and L. Sun, *Nat. Catal.*, 2024, **7**, 944–952.
57 W. Sun, X. Zheng, X. Zheng, M. Gao, Y. Liu and H. Pan, *Angew. Chem., Int. Ed.*, 2025, e202422062.